Joining Aluminum Alloy to Steel by Resistance Projection-Plug Welding

Kexu Ren, Ranfeng Qiu, Hengbo Ma, and Hongxin Shi

In order to improve the joining performance between aluminum alloy and steel, a method termed resistance projection-plug welding was tried to weld steel to aluminum alloy. The microstructure and properties of the joint obtained by this method under various welding parameters were analyzed. Scanning electron microscopy studies of the interfacial microstructures revealed that a reaction layer, consisting of Fe_2Al_5 adjacent to steel and $FeAl_3$ adjacent to aluminum alloy, is formed in the interface outside the nugget. The maximum tensile shear and cross-tension loads of the joint reached 6.92 and 4.13 kN, respectively, in comparison with 5.0 and 1.4 kN, respectively, for resistance spot welding with a cover plate. The results revealed that the resistance projection-plug welding is an effective method for welding steel and aluminum alloys.

1. Introduction

To reduce greenhouse gas emission and protect the environment, lightweight automobiles are required in the automotive industry. Partially replacing steels in the steel-dominated body-in-white with light materials, such as aluminum alloy, is an effective strategy for reducing vehicle weight (Ref 1). Resistance spot welding (RSW) is a primary welding process used in the traditional automobile body because of advantages such as high production efficiency, simple operation, no filling materials, and easy automation (Ref 2). Although RSW between aluminum alloy and steel is necessary, it is becoming a challenging issue because there are considerable differences in melting point, specific heat, thermal conductivity, electrical resistivity, linear expansion coefficient, and metallurgical compatibility between these materials (Ref 3, 4), which attracted the attention of a large number of researchers.

Studies on RSW between aluminum alloy and steel can be summarized into the following three main aspects: the use of cover plate or special electrodes, the employment of intermediate transition layer, and the introduction of a rivet in the joint. In the approach using cover plate or special electrodes, the main purpose of the studies is to balance the heat on both sides of aluminum alloy and steel and optimize the welding temperature

field (Ref 5-9). The results show that the application of the cover plate (belt) increases the size of the nugget and the tensile shear load and also extends the service life of the electrode (Ref 5-7). Sun and Zhang et al. used a spherical tip electrode on the aluminum alloy side and a planar circular tip electrode on the steel side to control the welding current path (Ref 8, 9). Their results show that the joint performance can be improved (Ref 8, 9). However, a thick intermetallic compound layer was formed at the welding interface (particularly in the center of the welding zone), which resulted in the lower cross-tension strength of the joint (Ref 10).

Regarding the solution that adopts the intermediate transition layer, Ibrahim et al. used Al-Mg alloy with lower melting point as an intermediate layer to weld A6061 aluminum alloy and stainless steel (Ref 11). Watanabe et al. considered that Mg in aluminum alloys could promote the Al-Fe reaction, and selected pure aluminum (A1050) as intermediate layer to weld A5052 aluminum alloy and SS400 steel (Ref 12). Chen reported the microstructure and tensile shear strength of the joint between A5052 aluminum alloy and DP600 steel welded by RSW with a Zn slice interlayer (Ref 13). Similarly, the filler of Al-Si was also used in the intermediate layer for RSW between aluminum alloy and steel to improve joint performance (Ref 14, 15). However, the addition of an intermediate transition layer cannot inhibit the formation of an intermetallic compounds layer at the welding interface; it only makes the layer thickness slightly thinner or forms other types of intermetallic compounds.

In recent years, the RSW between aluminum alloy and steel has been performed with an auxiliary rivet to strengthen the performance of the joint. In the studies of Qiu et al., a steel rivet was first inserted into a hole drilled beforehand in the aluminum alloy sheet and then welding was performed using an RSW machine (Ref 16). Coincidentally, Ling et al. used a steel rivet with end cap to weld aluminum alloy and steel using a process of resistance element welding (Ref 17, 18). The mechanization of the rivet insertion can be enhanced by the use of some hybrid joining methods, such as RSW and self-piercing riveting (Ref 19), RSW and friction element welding (Ref 20), RSW and riveting (Ref 21). The main load-bearing interface of the joint welded by these welding methods can vary from the aluminum/

Kexu Ren and Hengbo Ma, School of Materials Science and Engineering, Henan University of Science and Technology, Luoyang 471039, China; and Collaborative Innovation Center of Nonferrous Metals, Luoyang 471039 Henan Province, China; and Ranfeng Qiu and Hongxin Shi, School of Materials Science and Engineering, Henan University of Science and Technology, Luoyang 471039, China; and Henan Key Laboratory of Non-ferrous Materials Science and Processing Technology, Luoyang 471003, China. Contact e-mail: qrftougao@163.com.

steel interface to the steel/steel interface, reducing the influence of interfacial intermetallic compounds on the joint performance. However, this type of process introduces a challenge to the equipment configuration of existing body production lines. Therefore, further research is needed in the integration of riveting and welding equipment to meet the requirements of engineering applications.

In view of the exposed, RSW between aluminum alloy and steel still needs further study. Combining the advantages of the RSW with cover plate and RSW with an auxiliary rivet, a joining method termed resistance projection-plug welding (RPPW) was proposed for welding aluminum alloy to steel. For welding aluminum alloy and steel by use of the method, it is required that a hole is drilled in the aluminum alloy sheet and a projection is punched in the steel cover plate. In the welding process, the aluminum alloy sheet was placed between a steel sheet and the cover plate where the projection was inserted into the hole, and then welding was done using a resistance spot welding machine. As thus, the formation of a nugget between steel and the cover plate of steel would be achieved due to their direct contact during welding; then, the performance of the joint would be improved. In the present study, aluminum alloy sheet and low-carbon steel sheet were welded by the use of the method. The microstructure and properties of the joint obtained by this method under various welding parameters were analyzed.

2. Experimental Procedures

The materials used for this study were a 2-mm-thick A6061 aluminum alloy sheet and a 1-mm-thick Q235 steel sheet. Their chemical compositions are given in Table 1. Aluminum alloy and steel sheets were cut into samples of 100 mm × 30 mm. Q235 steel sheet pieces of 30 mm × 30 mm × 1 mm were used as cover plate.

A projection of 2 mm height was punched in the center of the cover plate, as shown in Fig. 1(a). A hole was drilled at the center of the overlap area of the A6061 sheet. Two types of specimens were assembled for tensile shear and cross-tension tests, as shown in Fig. 1(b) and (c), respectively. As shown in Fig. 1, the steel sheet was overlapped with the A6061 sheet with the prefabricated hole, the cover plate was placed on the top of the aluminum alloy sheet, and its projection was inserted into the hole. Welding was implemented on the projection using a stationary DC spot welding machine. Electrodes with a tip diameter of 6 mm were used. Welding conditions are listed in Table 2. In the four groups of parameter combinations, the welding current, welding time, electrode force, and diameter of the hole were changed under other fixed conditions. Seven joints were welded per condition, of which five joints were used for tensile shear testing and two joints were used for cross section studies.

After welding, tensile shear and cross-tension tests of the joint were performed under a crosshead velocity of 2 mm/min at room temperature. The fractures of joint were observed and analyzed; phase analyses were performed by using an x-ray diffractometer (XRD) on the fracture of A6061 side. Some joints were used for microstructure observation. They were cut by mechanical cutting through the weld center, and their cross sections were ground and polished. The joints microstructures
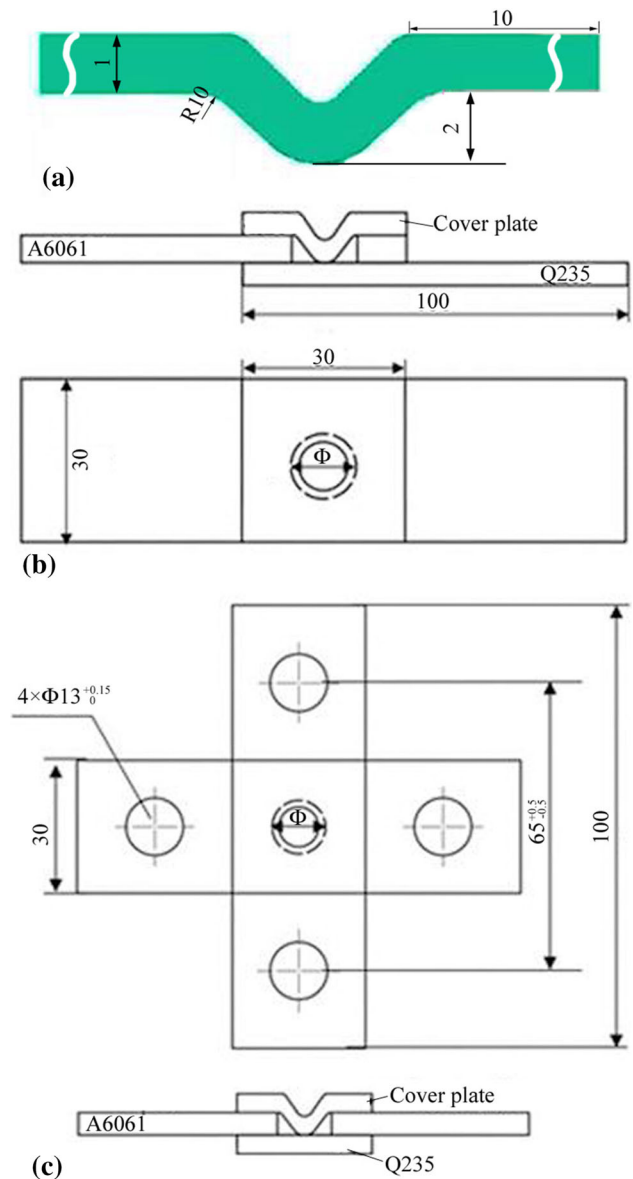

Fig. 1 Schematic of the cover plate (a), assembly diagram of specimen for the tensile shear test (b) and for the cross-tension test (c)

Table 1 Composition of parent metals (wt.%)

Materials	Fe	V	C	P	S	Mn	Si	Cr	Cu	Ti	Mg	Al
A6061	…	…	…	…	…	0.15	0.6	0.04	0.3	0.15	1.0	Bal.
Q235	Bal.	0.06	0.14	0.04	0.02	1.0	0.4	…	…	…	…	…

Table 2 Welding conditions

	Set 1	Set 2	Set 3	Set 4
Hole diameter, mm	9.0-11.0	10.0	10.0	10.0
Welding current, kA	12	8-16	12	12
Welding time, s	0.3	0.3	0.1-0.5	0.3
Electrode force, kN	3.1	3.1	3.1	2.1-4.1
Up-slope time, s	0.2	0.2	0.2	0.2
Down-slope time, s	0.2	0.2	0.2	0.2
Holding time, s	0.3	0.3	0.3	0.3

Fig. 2 Jigsaw puzzle of the joint cross section image and its schematic

were observed by the use of a scanning electron microscope (SEM) (JSM-5610LV) equipped with energy-dispersive x-ray spectroscopy (EDS).

3. Results and Discussion

3.1 Macro-morphology and Microstructure of Joints

Figure 2 shows a jigsaw puzzle of the RPPW joint cross section image and its schematic, which was described according to the characteristics of the joint cross section. The joint was obtained under welding of 14 kA (condition of set 2). The following characteristics are exhibited on the cross section image of the joint. First, a nugget, which its cross section is oval-shaped, was formed between the cover plate and the parent metal of steel. During spot welding, the heating area is circular due to the circular shape of the electrodes used. Under the action of the electrode force, the molten metal in the welding zone expands to the surrounding area, especially in the interplate area. This caused that the cross section of nugget was oval-shaped. No evident macro-welding defects were observed in the nugget. This indicated that a reliable joining between them was achieved. Second, the process hole in the aluminum alloy sheet was completely filled by the nugget. Third, traces of melting were observed in the aluminum alloy adjacent to the nugget. That is, the aluminum alloy inside the fusion line melted during the welding process.

Figure 3(a) shows a typical metallographic image of the RPPW joint, which was taken from the position A in Fig. 2. Although the grains in the nugget and the heat-affected zone (HAZ) of the joint were larger than those in the base metal, no microscopic defects were found. Figure 3(b) and (c) shows the enhanced metallographic images of the HAZ (position R) and the nugget (position L) of the joint, respectively. As shown, the nugget was mainly composed of a pearlite-like structure and a small amount of a Widmanstatten structure with white contrast, whereas the heat-affected zone was composed of pearlite-like structure and ferrite. These microstructure characteristics indicate that the cover plate and the parent metal of steel melted and formed a nugget during the welding process; thus, metallurgical bonding between them was achieved.

Figure 4(a) shows a SEM image of the interfacial zone outside the nugget, which was taken from the position B in Fig. 2. As shown, the metallurgical joining was achieved in the interfaces of aluminum alloy and cover plate, aluminum alloy and parent metal of steel. The high-magnification images at the positions C, D, and E in Fig. 4(a) are shown in Fig. 4(b), (c) and (d), respectively. As sh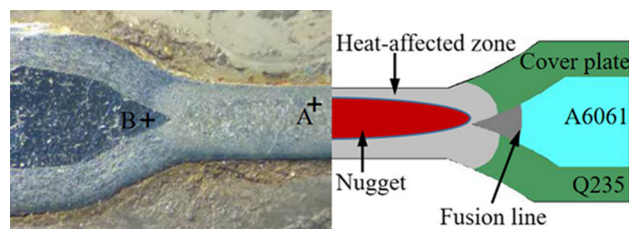own, a continuous reaction layer is observed in Fig. 4(b) and (c). The morphological characteristics of the reaction layer are consistent with those reported in previous studies (Ref 5, 16). Figure 4(e) shows the composition analysis results along the MN line in Fig. 4(b). There were two platforms in the composition distribution curve; the one adjacent to the steel was wider and the other near the aluminum side was narrower. The results of the quantitative component analysis at the positions F and G are listed in Table 3. According to the results, it can be inferred that the reactant of the adjacent steel was Fe_2Al_5 and that of the adjacent aluminum was $FeAl_3$. Figure 5 shows the XRD patterns from the fracture surface of A6061 side. As shown, intermetallic compounds of Fe_2Al_5 and $FeAl_3$ were detected from the fracture. This further confirms the above EDS analysis results. Therefore, the reaction layer consisted of Fe_2Al_5 adjacent to steel and $FeAl_3$ adjacent to aluminum alloy. This is also consistent with the results reported by Qiu et al. (Ref 5).

By comparing Fig. 4(b) and (c), it is observed that the thickness of the reaction layer at the welding interface is different. The reaction layer formed at position C was thicker than that formed at position D in Fig. 4(a). This is because the closer the position to the nugget, the longer the high-temperature interaction between Al and Fe at the welding interface. Similarly, as shown in Fig. 4(d), only few sporadic reactants were observed at the position E, outside the fuse line.

Moreover, the formation of a crack between the aluminum alloy and steel was remarkable, as shown in Fig. 4(d). This is considered to be due to the tensile stress perpendicularly applied to the interface during the welding process. Under the action of the electrode force, the steel and the cover plate on both sides of the process hole in the aluminum alloy were compressed and in close contact. In this case, the steel plate acted as a lever, whose fulcrum was the aluminum alloy around the process hole. Thus, the steel outside the welding zone was subjected to tensile stress perpendicular to the interface during the welding process. The larger the distance from the welding zone, the larger the upwarp of steel sheet from the aluminum alloy plate. Far from the fusion line, the crack propagated along the interface between steel and aluminum, as shown in Fig. 4(d). This implies that the joining between steel and aluminum alloy was not achieved. In contrast, near the fusion line, the crack propagated within the aluminum alloy, as shown in Fig. 4(d). The crack is considered to have formed during the holding phase. Under the action of the electrode force, the aluminum alloy around the process hole thinned during the heating phase. This led to the aluminum alloy adjacent to the fusion line (nearby position E) to contact with the steel; the metallurgical reaction occurred, and the reactants were formed at the interface. Near the position, the joining between steel and aluminum alloy was achieved. After the welding current stopped, the nugget metal with a high melting point solidified
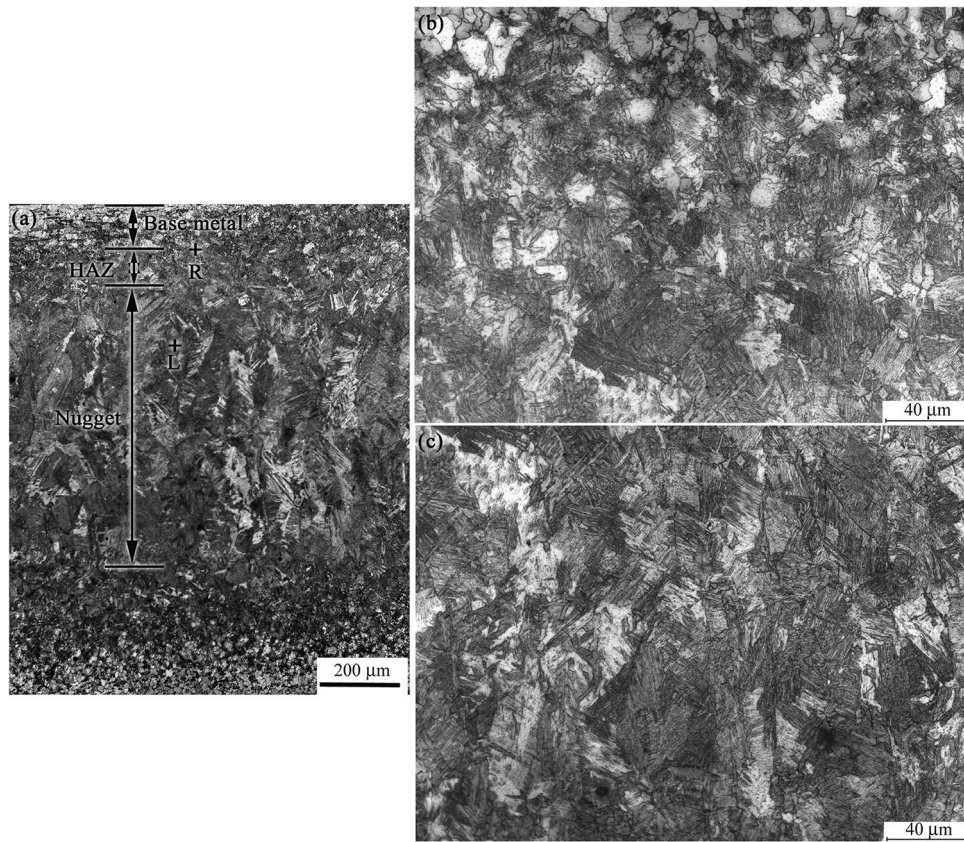
Fig. 3 Microstructure of the joint, (a) welding zone, (b) HAZ, (c) nugget
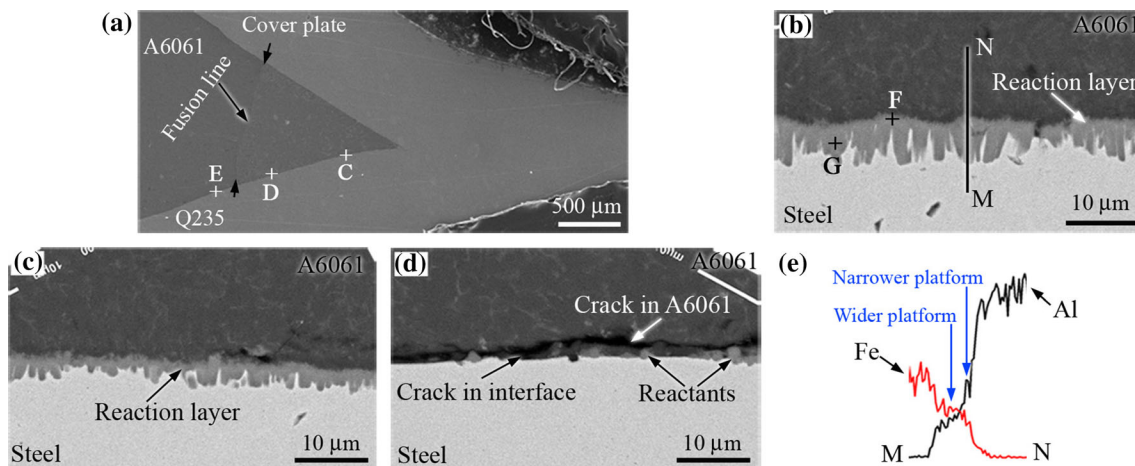

Fig. 4 Microscopic morphology of position B (in Fig. 2) and EDS results, (a) image of interfacial zone, (b), (c) and (d) images at the positions C, D, and E, respectively, (e) EDS results

Table 3 EDS analysis results at the locations in Fig. 4 and 11 (at.%)

Elements	F	G	H	J	K
Fe	30.48	29.77	29.07	97.74	93.98
Al	69.52	70.23	70.93	2.26	6.02

first; and it sustained the electrodes. Meanwhile, the cooling shrinkage of the aluminum alloy outside the fusion line caused the formation of a crack. Due to the formation of hard and brittle intermetallic compounds at the interface, the stress concentration occurred in the aluminum alloy near the interface. Consequently, the crack extended in the aluminum alloy. Similar phenomena were also observed in the joints obtained under other welding conditions.

According to the mentioned results, the forming process of the RPPW joint between aluminum alloy and steel (henceforth called RPPW joint of A6061/steel) is illustrated in Fig. 6, in which Fig. 6(a), (b), (c), (d), and (e) represents the schematic of the joint formation and Fig. 6(f), (g), (i), and (j) represents the stage of occurrence. The assembly sample was placed between

the upper and lower electrodes, as shown in Fig. 6(a), when the electrodes were aligned with the projection and process hole. During squeeze phase, as shown in Fig. 6(g), the cover plate was contacted with the steel in the process hole due to its plastic deformation under the action of the electrode force, as shown in Fig. 6(b). When the welding current was activated for heating, the plastic deformation of the cover plate and steel sheet further increased, so that the process hole was filled with them. At the same time, a nugget was formed between them, and the aluminum alloy around the process hole was melted by the heat conduction shown in Fig. 6(c). As the heat continued, the nugget and melted aluminum alloy zone further expanded, as shown in Fig. 6(d). During the holding phase, the nugget and the melted aluminum alloy were cooled and solidified to form the joint, as shown in Fig. 6(e).

3.2 Mechanical Properties of Joints

Figure 7 shows the effect of the process hole's diameter on the tensile shear load (TSL) and cross-tension load (CTL) of the RPPW joint of A6061/steel. As shown, with the increase in the process hole's diameter, the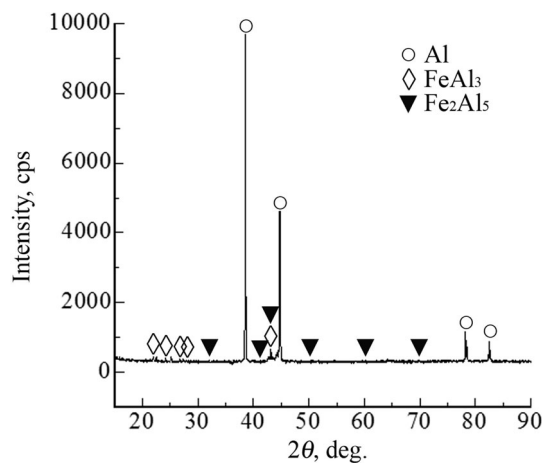 TSL and CTL of the RPPW joint of A6061/steel initially increased and then decreased. When the diameter of the process hole was 10 mm, the TSL and CTL of the RPPW joint reached the maximum values, 5.51 and 3.24 kN, respectively. When the diameter of the process hole was small, the cover plate and steel sheet could not be fitted together in a large area, and the aluminum alloy around the process hole hindered the nugget growth. However, when the diameter of the process hole was too large, it could not be fully filled. This resulted in stress concentration at the aluminum alloy around the process hole during the tensile testing, which led to the performance degradation of the joint.

Figure 8 shows the effect of the welding current on the TSL and CTL of the RPPW joint of A6061/steel. In the welding current range from 8 to 14 kA, the TSL and CTL of the joint increased with the increase in welding current. When the welding current was 14 kA, they reached the maximum values of 6.92 and 4.13 kN, respectively. When the welding current exceeded 14 kA, the performance of the joint slightly decreased with the increase in welding current. This is because more heat was generated in the weld zone with the increase in welding current, which resulted in a larger nugget. However, considerable welding current can cause the nugget metal to overheat
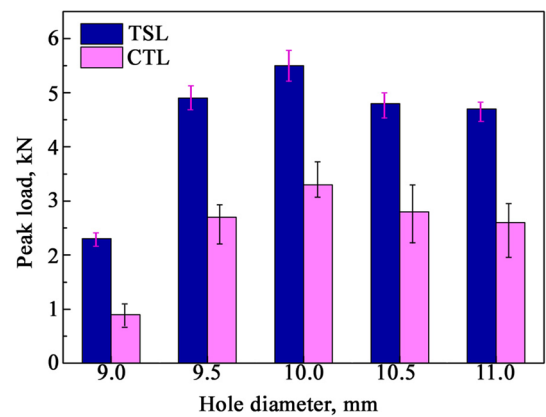

Fig. 5 XRD patterns

Fig. 7 Effect of the process hole's diameter on the TSL and CTL of the RPPW joint of A6061/steel
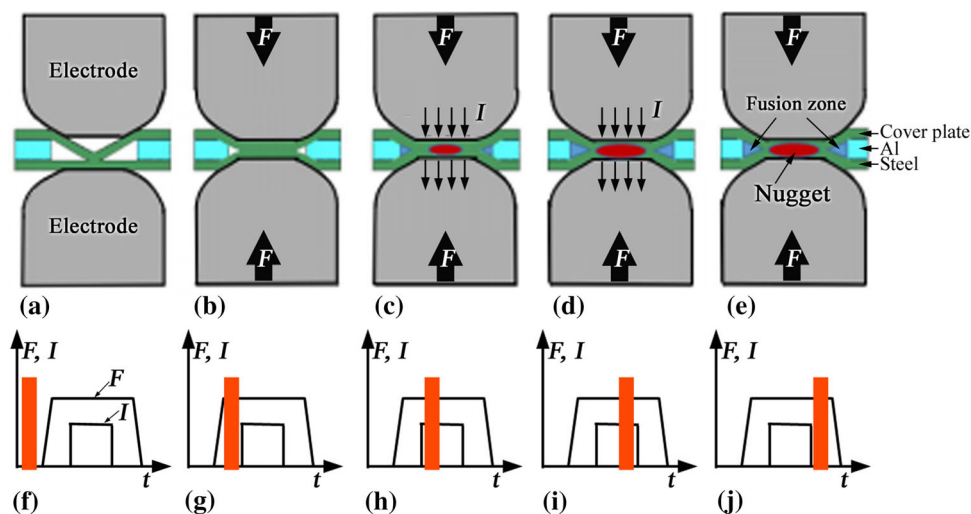

Fig. 6 Schematic of the forming process of the RPPW joint, (a) and (f) before welding, (b) and (g) squeeze phase, (c) and (d) first half of welding, (d) and (i) latter half of the welding, (e) and (j) holding phase
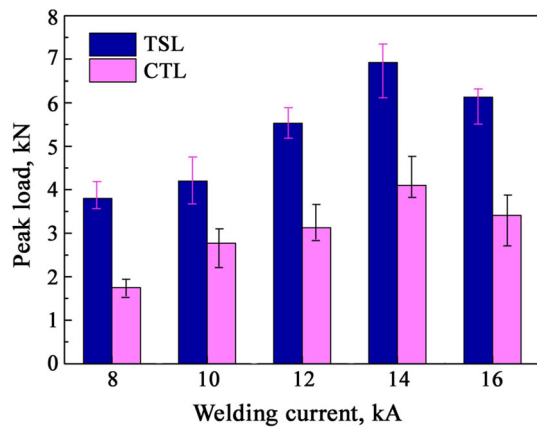
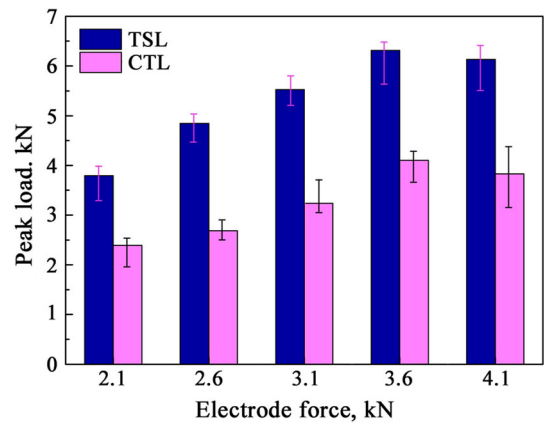**Fig. 8** Effect of welding current on the TSL and CTL of the RPPW joint of A6061/steel
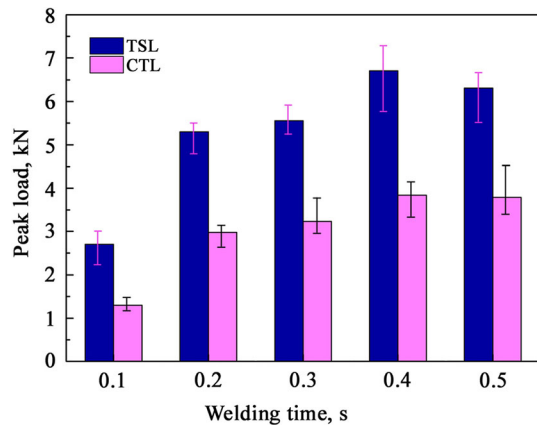

Fig. 9 Effect of welding time on the TSL and CTL of the RPPW joint of A6061/steel

during the welding and form more Widmanstatten structure, which can affect the performance of the joint. This is considered to be the reason for the poor performance of the joint in the high welding current range, as shown in Fig. 8.

Similarly, the TSL and CTL of the RPPW joint also initially increased and then decreased with the extension of welding time, as shown in Fig. 9. When the welding time was 0.4 s, they reached the maximum. The reason is similar to the effect of the welding current, because the heat generated in the welding zone is proportional to the welding time and the square of the welding current.

The relationship between the TSL and CTL of the RPPW joint of A6061/steel and the electrode force is shown in Fig. 10. In the electrode force range from 2.1 to 3.6 kN, the TSL and CTL of the joint increased with the increase in electrode force. When the electrode force was 3.6 kN, they reached the maximum values of 6.35 and 4.11 kN, respectively. When the electrode force exceeded 3.6 kN, the TSL and CTL of the joint slightly decreased with the increase in the electrode force. This is because increasing the electrode force can make the contact area between the cover plate and the steel expand, and promote the enlargement of the nugget. In the range of low electrode force, the mechanical performance of the joint improved with the increase in the electrode force. However,

Fig. 10 Effect of electrode force on the TSL and CTL of the RPPW joint of A6061/steel

excessive electrode force can cause the welding zone to become thinner, which degrades the TSL and CTL of the joint.

For both tensile shear testing and cross-tension testing, the fracture mode of the RPPW joints obtained in the study was mainly plug-type fracture. Figure 11 shows the macroscopic and microscopic fractures of the joint after tensile shear failure. The joint was obtained under welding of 12 kA (condition of set 2). As can be seen from Fig. 11(a), (b), and (c), the welding zone was drawn from the Q235 side, leaving a button-shaped nugget on the side of the cover plate. Three characteristic zones were observed at the fracture of the cover plate. First, the outer part of the fracture was a banded zone with bright contrast, marked as P in Fig. 11(c). A larger view of this zone is shown in Fig. 11(d). The EDS results at the position H are also listed in Table 3. According to the results, it can be inferred that the joint was broken from Fe-Al intermetallic compounds in the zone. Figure 11(e) shows a SEM image taken from the position Q in Fig. 11(c). As shown, there were two characteristic zones, the U region next to the button and the V region close to the P zone. Some dimples were observed in the V region, whereas laceration morphologies were observed in the U region. The EDS results at the positions K and J listed in Table 3 indicate that the joint was broken from the steel in both regions. Moreover, the bright white contrast in the U region indicates that the relative position of the region is higher.

According to the mentioned results, the failure process of the RPPW joint of A6061/steel during tensile shear testing is illustrated in Fig. 12. Due to the additional torque generated during tensile shear testing, the welding interface was subjected to the forces in parallel and near vertical directions (Ref 22). Thus, the fracture cracks originated from the weld edges S and S′ (shown in Fig. 12), at the outer edge of the welding zone. The crack propagated along the Al/steel interface, where the intermetallic compounds were formed; with loading, it entered the interfacial zone between the cover plate and steel. As the additional torque increased, the crack expanded to T and T′, where the stress concentration was larger during the tensile shear testing, and then the joint broke. Here, the P′, U′, and V′ regions are considered to correspond to the P, U, and V regions in the fracture, respectively, as shown in Fig. 11(c) and (e).

Figure 13 shows a load–displacement curve of the joint, of which fractures are shown in Fig. 11. From the load–displacement curve and fracture of the joint, the failure of the RPPW joint of A6061/steel was mainly a ductile fracture. Similar
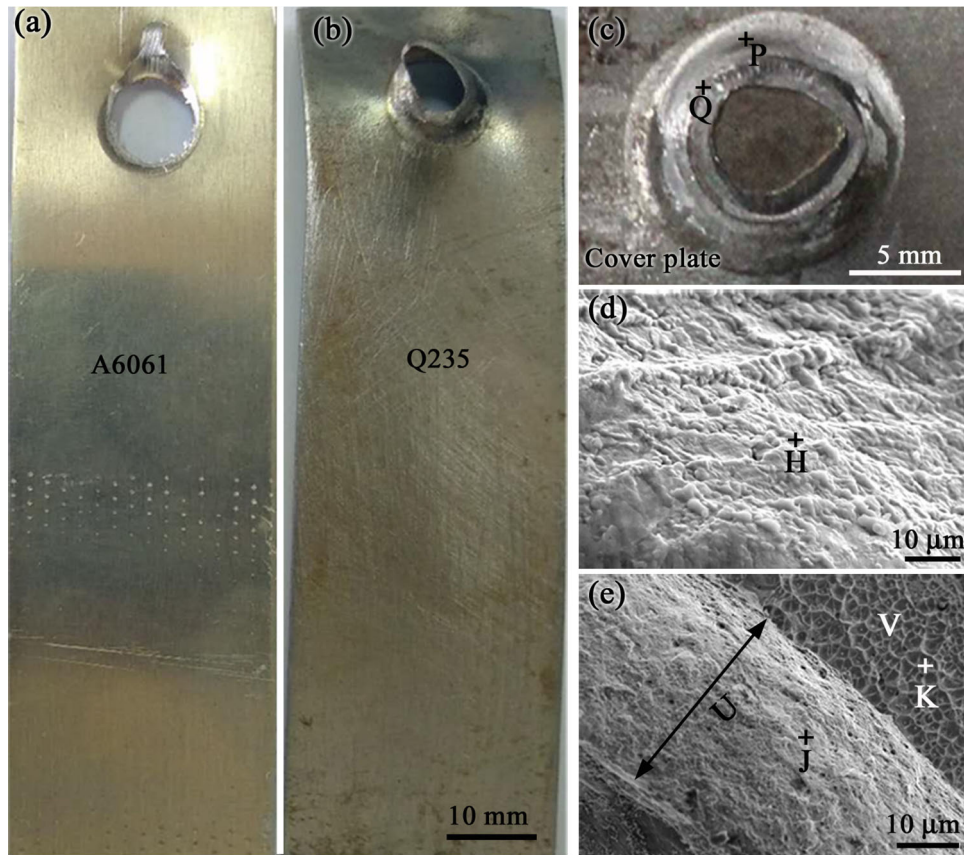
Fig. 11 Macroscopic and microscopic fractures of the joint after tensile shear failure, (a) A6061 side, (b) Q235 side, (c) cover plate, (d) microscopic fracture of Q region
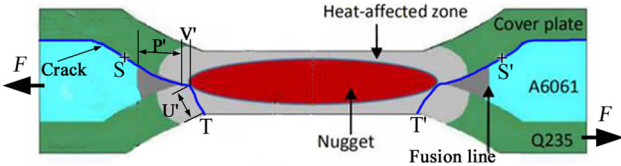

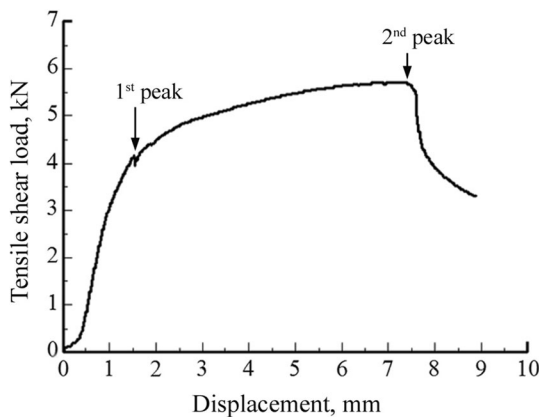**Fig. 12** Schematic of the joint failure during tensile shear testing

Fig. 13 Load–displacement curve of the RPPW joint of A6061/steel

results were obtained for other joints obtained in this study. Compared with the joint of aluminum alloy and steel welded by RSW with a rivet (Ref 16), the RPPW joint of A6061/steel has

higher tensile shear load and higher absorption energy. Furthermore, the load–displacement curve of the RPPW joint exhibits two peaks: The first peak was the failure of the Al/steel interface, and the second was the fracture of the spot weld of steel.

In the previous study, the maximum TSL and CTL of the joint between aluminum alloy and steel welded by RSW with a cover plate reached 6.68 and 0.55 kN, respectively (Ref 10, 23). In the study of Chen et al. (Ref 24), a 1.2-mm-thick aluminum alloy (AA6022-T4) and 2-mm-thick hot-dip galvanized low-carbon steel were welded by us of traditional resistance spot welding. The maximum TSL and CTL of the joint between aluminum alloy and steel welded by RSW with a cover plate reached 5.0 and 1.4 kN, respectively (Ref 24). In comparison with these results, the joints in the present study revealed higher TSL and CTL, as shown in Fig. 7, 8, 9, and 10. Previous studies reveal that the failure of resistance spot-welded joint between aluminum alloy and steel occurred from the joining interface of Al/steel or the aluminum alloy sheet during tensile shear testing (Ref 13, 23, 24). The RPPW joints of A6061/steel obtained in this study were eventually fractured from the steel sheet during tensile shear testing as previously mentioned. This is because a nugget of steel was formed in the RPPW joints of A6061/steel, whereas the interface of Al/steel intersected the joint between aluminum alloy and steel welded by the use of traditional resistance spot welding. As thus, the main bearing interface of RPPW joints changed from the aluminum/steel interface to the steel/steel interface; then, the performance of joint between aluminum alloy and steel can be

improved by use of RPPW method. Therefore, the microstructure and size of nugget are the main factors affecting the performance of RPPW joints of A6061/steel. Conversely, the interface of Al/steel outside the nugget, which is marked by P′ in Fig. 12, has a little effect on the performance of RPPW joints of A6061/steel and can affect the value of the first peak load as shown in Fig. 13.

4. Conclusions

Resistance projection-plug welding between steel sheet and aluminum alloy sheet was experimentally investigated here as a possible joining technology for the manufacturing of lightweight body-in-white. Results were assessed by means of transversal tensile and SEM.

The RPPW joint of A6061/steel comprises a nugget of steel and joining zone of Al/steel outside the nugget. The reaction products of Fe_2Al_5 and $FeAl_3$ were formed at the Al/steel interface outside the nugget.

The process hole prefabricated in the aluminum alloy sheet plays an important role in the performance of the RPPW joint of A6061/steel. Smaller process hole can hinder the nugget growth; larger process hole cannot be fully filled by the nugget.

The TSL and CTL of the RPPW joint of A6061/steel initially increased and then decreased with the increase in welding current, welding time, and electrode force. The maximum TSL and CTL of the RPPW joint of A6061/steel reached 6.92 and 4.13 kN, respectively. These have been greatly improved in comparison with that of the Al/steel joint welded by us of traditional resistance spot welding.

Overall, from the present results, RPPW is an effective method for joining steel and aluminum alloy due to the change in the main bearing interface of the joint from the aluminum/steel interface to the steel/steel interface.

References

1. H. Zhao, G. Zhang, Q. Zhang, C. Zhang, and Y. Li, Joining Mechanism and Mechanical Properties of Metallic Bump Assisted Weld-Bonded (MBaWB) Joints of AA6061-T6 and Bare DP590, *J. Manuf. Process.*, 2020, **50**, p 204–215

2. Y. Zhang and D. Sun, Microstructures and Mechanical Properties of Steel/Aluminum Alloy Joints Welded by Resistance Spot Welding, *J. Mater. Eng. Perform.*, 2017, **26**(6), p 2649–2662

3. S. Meco, S. Ganguly, S. Williams, and N. McPherson, Effect of Laser Processing Parameters on the Formation of Intermetallic Compounds in Fe-Al Dissimilar Welding, *J. Mater. Eng. Perform.*, 2014, **23**(9), p 3361–3370

4. H. Xia, C. Tan, L. Li, and N. Ma, In Situ SEM Observations of Fracture Behavior of Laser Welded-Brazed Al/Steel Dissimilar Joint, *J. Mater. Eng. Perform.*, 2018, **27**(9), p 1047–1057

5. R. Qiu, H. Shi, K. Zhang, Y. Tu, C. Iwamoto, and S. Satonaka, Interfacial Characterization of Joint Between Mild Steel and Aluminum Alloy Welded by Resistance Spot Welding, *Mater. Charact.*, 2010, **61**(7), p 684–688

6. J.S. Kim, I.J. Kim, and Y.G. Kim, Optimization of Welding Current Waveform for Dissimilar Material with DP590 and Al5052 by Delta-Spot Welding Process, *J. Mech. Sci. Technol.*, 2016, **30**(6), p 2713–2721

7. Y. Che, L. Wang, D. Sun, H. Li, and W. Geng, Microstructures and Mechanical Properties of Resistance Spot-Welded Steel/Aluminum Alloy Joints with Process Tapes, *J. Mater. Eng. Perform.*, 2018, **27**(10), p 5532–5544

8. D. Sun, Y. Zhang, Y. Liu, X. Gu, and H. Li, Microstructures and Mechanical Properties of Resistance Spot Welded Joints of 16Mn Steel and 6063-T6 Aluminum Alloy with Different Electrodes, *Mater. Des.*, 2016, **109**, p 596–598

9. W. Zhang, D. Sun, L. Han, and Y. Li, Optimised Design of Electrode Morphology for Novel Dissimilar Resistance Spot Welding of Aluminium Alloy and Galvanised High Strength Steel, *Mater. Des.*, 2015, **85**, p 461–470

10. R. Qiu, S. Satonaka, and C. Iwamoto, Effect of Interfacial Reaction Layer Continuity on the Tensile Strength of Resistance Spot Welded Joints between Aluminum Alloy and Steels, *Mater. Des.*, 2009, **30**, p 3686–3689

11. I. Ibrahim, R. Ito, T. Kakiuchi, Y. Uematsu, K. Yun, and C. Matsuda, Fatigue Behaviour of Al/Steel Dissimilar Resistance Spot Welds Fabricated Using Al-Mg Interlayer, *Sci. Technol. Weld. Join.*, 2016, **21**(3), p 223–233

12. T. Watanabe, Y. Doi, A. Yanagisawai, and S. Konuma, Resistance Spot Welding of Mild Steel to Al-Mg Alloy, *Q. J. Jpn. Weld. Soc.*, 2005, **23**(3), p 491–495

13. J. Chen, X. Yuan, Z. Hua, T. Li, K. Wu, and C. Li, Improvement of Resistance-Spot-Welded Joints for DP 600 Steel and A5052 Aluminum Alloy with Zn Slice Interlayer, *J. Manuf. Process.*, 2017, **30**, p 396–405

14. W. Zhang, D. Sun, L. Han, and D. Liu, Interfacial Microstructure and Mechanical Property of Resistance Spot Welded Joint of High Strength Steel and Aluminium Alloy with 4047 AlSi12 Interlayer, *Mater. Des.*, 2014, **57**, p 186–194

15. G. Zhang, H. Zhao, X. Xu, G. Qiu, Y. Li, and Z. Lin, Metallic Bump Assisted Resistance Spot Welding (MBaRSW) of AA6061-T6 and Bare DP590: Part II-Joining Mechanism and Joint Property, *J. Manuf. Process.*, 2019, **44**, p 19–27

16. R. Qiu, N. Wang, H. Shi, L. Cui, L. Hou, and K. Zhang, Joining Steel to Aluminum Alloy by Resistance Spot Welding with A Rivet, *Int. J. Mater. Res.*, 2015, **106**(1), p 60–65

17. Z. Ling, Y. Li, Z. Luo, Y. Feng, and Z. Wang, Resistance Element Welding of 6061 Aluminum Alloy to Uncoated 22MnMoB Boron Steel, *Mater. Manuf. Process.*, 2016, **31**(16), p 2174–2180

18. Z. Ling, Y. Li, Z. Luo, S. Aon, Z. Yin, Y. Gu, and Q. Chen, Microstructure and Fatigue Behavior of Resistance Element Welded Dissimilar Joints of DP780 Dual-Phase Steel to 6061-T6 Aluminum Alloy, *Int. J. Adv. Manuf. Technol.*, 2017, **92**, p 1923–1931

19. M. Lou, Y. Li, Y. Wang, B. Wang, and X. Lai, Influence of Resistance Heating on Self-Piercing Riveted Dissimilar Joints of AA6061-T6 and Galvanized DP590, *J. Mater. Process. Technol.*, 2014, **214**, p 2119–2126

20. J.P. Oliveira, K. Ponder, E. Brizes, T. Abke, A.J. Ramirez, and P. Edwards, Combining Resistance Spot Welding and Friction Element Welding for Dissimilar Joining of Aluminum to High Strength Steels, *J. Mater. Process. Technol.*, 2019, **273**, p 116–192

21. X. Fang and F. Zhang, Hybrid Joining of A Modular Multi-Material Body-in-White Structure, *J. Mater. Process. Technol.*, 2020, **275**, p 116351

22. S. Satonaka, K. Kaieda, and S. Okamoto, Prediction of Tensile-Shear Strength of Spot Welds Based on Fracture Modes, *Welding in the World*, 2004, **48**(5/6), p 39–45

23. R. Qiu, C. Iwamoto, and S. Satonaka, Interfacial Microstructure and Strength of Steel/Aluminum Alloy Joints Welded by Resistance Spot Welding with Cover Plate, *J. Mater. Process. Technol.*, 2009, **209**, p 4186–4193

24. J. Chen, Z. Feng, H.P. Wang, B.E. Carlson, T. Brown, and D. Sigler, Multi-Scale Mechanical Modeling of Al-Steel Resistance Spot Welds, *Mater. Sci. Eng., A*, 2018, **735**, p 145–153